Microporous and Mesoporous Materials 253 (2017) 55–63

Contents lists available at ScienceDirect

Microporous and Mesoporous Materials

journal homepage: www.elsevier.com/locate/micromeso

A novel strategy to enhance hydrothermal stability of Pd-doped organosilica membrane for hydrogen separation

Jiaojiao Lei [a], Huating Song [a], Yibin Wei [a, b], Shuaifei Zhao [b], Hong Qi [a, *]

[a] State Key Laboratory of Material-Oriented Chemical Engineering, Membrane Science and Technology Research Center, Nanjing Tech University, Nanjing 210009, Jiangsu, China
[b] Department of Environmental Sciences, Macquarie University, Sydney, NSW 2109, Australia

ARTICLE INFO

Article history:
Received 8 March 2017
Received in revised form
15 June 2017
Accepted 20 June 2017
Available online 21 June 2017

Keywords:
Metal doping
Organosilica membrane
Hydrothermal stability
Steam atmosphere
Gas separation

ABSTRACT

Pd-doped organosilica (POS) membranes are calcined in N_2 and steam atmospheres for hydrogen separation. Chemical compositions and microstructures of the membranes are characterized by X-ray photoelectron spectroscopy (XPS), transmission electron microscopy (TEM), Fourier transform infrared spectra (FTIR) and N_2 absorption-desorption measurement. Gas separation performances and hydrothermal stabilities of the membranes are also evaluated and compared. The membrane calcined in steam atmosphere (i.e. POS-S membrane) shows a high H_2 permeance (2.5×10^{-7} mol·m^{-2}·s^{-1}·Pa^{-1}) and H_2/CO_2 permselectivity (9.2, doubles the Knudsen diffusion factor 4.69). Notably, compared with the POS membrane calcined in N_2, the POS-S membrane displays more excellent hydrothermal stability throughout a 190-h test, which is superior to most silica-derived membranes reported. The significantly enhanced hydrothermal stability is mainly attributed to the low content of unstable moieties in the POS network after steam calcination. Steam conditions make unstable intermediate Pd oxide transfer into stable PdO and reduce content of inorganic moieties during the calcination, leading to high hydrothermal stability of the membrane. Therefore, calcination in steam atmosphere may offer an effective strategy to develop desirable POS membranes with high separation performances and excellent hydrothermal stabilities for practical hydrogen separation.

1. Introduction

Fossil fuel exhaustion, environment pollution and climate change are critical challenges we are facing today. Hydrogen as a major clean energy carrier for versatile applications has gained a great portion of research efforts [1,2]. Since there is no natural hydrogen resource available, highly efficient hydrogen production routes are keen to be developed. Methane steam reforming (MSR) and water gas shift (WGS) reactions are well-established methods to generate hydrogen on a large scale that currently produce more than 95% of hydrogen in the US [3]. However, to improve the conversion of these reactions, many technical challenges, particularly efficient H_2 separation and purification, are yet to be solved.

To date, numerous membranes have been used for hydrogen separation and purification. Zeolite membranes usually show both excellent hydrothermal stability and chemical stability owing to their unique crystalline nature, particularly the MFI-type zeolite membrane. However, the H_2 permeance of zeolite membrane is still required to improve [4,5]. In recent year, the emerging MOF materials, serving as a new type of separation material, have received remarkable attentions due to their unprecedented properties, such as high surface area, abundant easy-to-functionalize cavities, chemical and thermal stability, and permanent porosity [6–10]. MOFs membranes have proved its feasibility in the field of H_2 separation since the H_2 permeance of could be reached up to 10^{-6} mol·m^{-2}·s^{-1}·Pa^{-1} [5,11,12]. Besides, novel two-dimensional nanomaterials, such as graphene oxide (GO), have also been fabricated as membrane materials for gas separation [13]. For example, Guan et al. [14] reported a ceramic-supported GO membrane through layer-by-layer evaporation spraying assembly. Although the H_2/CO_2 selectivity of the prepared membranes could reach up to 20.9, the best H_2 permeance of the membrane was 2.7×10^{-8} mol·Pa^{-1}·m^{-2}·s^{-1}. Notably, it is well-known that GO is not thermally durable at temperature above 100 °C and thus GO membranes with excellent hydrothermal stability is more challenging for its practical application.

* Corresponding author.
E-mail address: hqi@njtech.edu.cn (H. Qi).

http://dx.doi.org/10.1016/j.micromeso.2017.06.041
1387-1811/

In additions, ceramic membranes based on silica, zirconia or titania, have been considered promising for gas separation in various industrial processes. Among these, microporous silica membranes prepared by sol-gel method exhibit great potential in sieving H_2 due to their unique porous networks. However, microporous silica networks are unstable in harsh environments, particularly in hot steam conditions. Attacked by water vapor, siloxane groups (i.e. Si-O-Si groups) is easily to be dissociated, resulting in the formation of mobile siloxane groups [15]. The mobile siloxane groups are subsequently condensed, leading to structural rearrangement of silica, which further limits the permeance and selectivity of membranes [16,17]. To improve H_2 separation performance and the resistance of silica membranes to water vapor, two stages including sol synthesis and thermal treatment in fabrication of microporous silica membranes can be optimized.

In sol synthesis, researchers attempted several new silica precursors (e.g. organosilica) to replace conventional tetraethoxysilane (TEOS) to prepare high performance microporous membranes. Organosilica membranes based on bis(triethoxysilyl)ethane (BTESE) with Si-C-C-Si bonds in the silica matrix are highly hydrothermal stability due to the more hydrophobic atomic network shielding siloxane groups from water vapor [18–20]. Second, doping metals such as Ni, Co, Zr, Pd and Nb into silica networks can also prevent network structure from densification in steam atmosphere [21–24]. Using BTESE as the precursor, we reported a Nb-BTESE derived hybrid silica membrane with a H_2 permeance of 6.28×10^{-8} $mol \cdot m^{-2} \cdot s^{-1} \cdot Pa^{-1}$, a H_2/CO_2 permselectivity of 108 and an outstanding stability after hydrothermal treatment [25]. Pd-doped organosilica (POS) membranes were found to be better than Nb-doped organosilica membranes in H_2 permeability and hydrothermal stability [24]. Doping Pd may affect the H_2 permeability and gas separation performance due to the high solubility of metal Pd for hydrogen atoms [22,26–29].

Optimization of thermal treatment conditions is another way to improve the performance of silica based membranes. Relevant parameters, such as calcination temperature, time and atmosphere have significant influences on the microstructures of silica membranes. Kanezashi et al. [30] proposed to calcine Ni-doped silica membranes at 550 °C in a water vapor environment to improve the membrane hydrothermal stability. After hydrothermal treatment for 60 h, the H_2 permeance of the membrane decreased to 2/5 of the initial value; while the H_2 permeance of the membrane calcined in air decreased drastically to 1/5 of the initial value after 38-h hydrothermal treatment. Similarly, Co-doped silica membrane calcined under a water vapor condition at 600 °C also exhibited a good hydrothermal stability when it exposed to 500 °C steam with partial pressure of 90 kPa [21]. Therefore, calcination in a steam condition may be an effective way to improve hydrothermal stabilities of silica based membranes.

In our previous work, incorporating Pd particles into organosilica structures resulted in enhanced hydrogen permeability of the organosilica membranes [24]. In this study, we investigate the effect of calcination conditions on the hydrogen permeability and hydrothermal stability of Pd-doped organosilica (POS) membranes. Two POS membranes were fabricated by calcination in N_2 and steam atmospheres at 400 °C. X-ray photoelectron spectroscopy (XPS), transmission electron microscopy (TEM), Fourier transform infrared (FTIR) spectroscopy and N_2 sorption measurements are used to investigate chemical and microstructure changes of the membranes (including powders that are considered as unsupported membranes). H_2 permeance and permselectivity of the POS membranes calcined in N_2 and steam atmospheres are evaluated and the mechanism of hydrothermal stability of the membranes is discussed.

2. Experimental

2.1. Chemicals and POS sol preparation

POS sols, based on 1, 2 - bis(triethoxysilyl)ethane (BTESE, purity = 97%) and palladium chloride ($PdCl_2$, purity > 98%), were prepared as reported elsewhere [24]. POS sols were finally obtained with a molar ratio of Pd: BTESE: EtOH: H_2O: HCl = 0.22: 1: 94.71: 55.55: 0.68.

2.2. Xerogel preparation and characterization

POS xerogels were prepared by drying the synthesized POS sols in petri dishes at ambient temperature for 12 h. Then the gels were ground into powders, and the powders were marked as POS-N and POS-S based on the thermal treatment conditions, i.e. N_2 atmosphere and steam atmosphere at 400 °C. The calcination procedure includes a heating process with a rate of 0.5 $°C \cdot min^{-1}$, heat preservation for 3 h at 400 °C and a cooling process with a rate of 0.5 $°C \cdot min^{-1}$. To prepare POS-S samples, the oven was filled with N_2 stream first, and then steam when the temperature was above 100 °C. N_2 stream was introduced again in the cooling process when the temperature was below 100 °C.

Hydrothermal treatment of POS powders was carried out in a hydrothermal reactor at 200 °C for 24 h. Appropriate quantity of water and 0.5 g POS powders were employed to ensure a saturated water vapor atmosphere in the reactor.

X-ray diffractometer (MiniFlex 600, Rigaku) with a Cu Kα radiation at 40 kV and 15 mA was used to identify the crystal structures of the powders. Fourier transform infrared (FTIR) spectra with a NICOLET 8700 (Thermo Nicolet Corporation) was used to determine chemical composition of the powders. An X-ray photoelectron spectrometer (XPS) equipped with a mono-chromatic Al Kα X-ray source (1486.6 eV) (ESCALAB250xi, Thermo Scientific) was used for elemental analysis of the powders. Morphological characteristics of the powders were imaged by transmission electron microscope (TEM, JEM-200CX, JEOL). N_2 adsorption-desorption isotherms at 373 K were performed with a physical gas adsorption instrument (ASAP 2020, Micromeritics) to evaluate microstructures of the powders. According to the cylindrical pore model, pore size distributions of the powders were estimated through the N_2 adsorption-desorption isotherms. Powders were degassed under vacuum at 473 K for 3 h before tests. Cross sectional images of the POS membranes were captured by scanning electron microscope (SEM, SU3500, HITACHI).

2.3. POS membrane fabrication and characterization

Home-made mesoporous γ-Al_2O_3 discs with pore diameters of 3–5 nm were used as the substrates. POS membranes were prepared by the dip-coating method in a clean room condition. Membrane fabrication was conducted using an automatic coating machine (Pervatech B.V., Netherland) at a withdraw speed of 12 mm s^{-1}. The coated membranes were first dried at 40 °C for 3 h in an oven. The POS-N and POS-S membranes were then calcined based on the same thermal treatments as described in Section 2.2.

Single gas permeances of POS-N and POS-S membranes were measured at 200 °C under a transmembrane pressure of 0.3 MPa using a dead-end mode apparatus. The membranes were tested using various gases with various kinetic diameters (d_k), starting from He (2.55 Å), H_2 (2.89 Å), CO_2 (3.3 Å), N_2 (3.64 Å), CH_4 (3.8 Å), to SF_6 (5.5 Å). The gas permselectivity, also known as ideal selectivity, was equal to the permeance ratio between two gases.

The H_2/CO_2 mixture gas separation was continuously monitored by a gas chromatograph (GC-2014, Shimadzu) equipped with a

thermal conductivity detector (TCD) and a packed column of Haysep DB (Alltech). An equivalent H_2/CO_2 gas mixture (60 cm^3/min) was first mixed and then introduced into the POS membrane side. The support side was swept by helium stream (30 cm^3/min).

Hydrothermal stabilities of the membranes were evaluated by measuring the single gas permeances before and after in-situ exposure to a gas mixture of N_2 and steam over a fixed period. Steam was generated by a steam generator attached to the gas permeation test apparatus. N_2 pressure was maintained at 0.3 MPa with a pressure gauge, and water vapor pressures were controlled at 100 kPa by carefully adjusting the steam temperatures at 99.6 °C. After hydrothermal treatment, the membranes were dried for 2 h with N_2 sweeping at 200 °C. Hydrothermal stability of the POS membranes was analyzed by repeating above-described single gas permeation tests throughout specified time intervals.

3. Results and discussion

3.1. POS powder characterization

Fig. 1 shows TEM images of the POS powders calcined at 400 °C in (a) N_2 and (b) steam atmospheres, respectively. Clear dark dots were observed from both samples, indicating that Pd has been successfully doped into the amorphous hybrid silica matrix. These Pd particles are randomly dispersed in the hybrid silica matrix with a size range between 2 and 10 nm. From the insets in Fig. 1a and b, we can see that the Pd particles in the POS-N powders are more homogeneous, while some Pd particles are clustered in the POS-S powders.

In Fig. 2, the characteristic peaks at around 3447, 2906, 1025 and 700 cm^{-1} are ascribed to Si-OH stretching, C-H stretching, Si-O-Si asymmetric stretching, and Si-C stretching vibrations, respectively [31]. C-H vibrations at 1274 and 1414 cm^{-1} correspond to ≡Si-CH_2-CH_2-Si≡ bond and suggest the presence of organic segment in the samples [32].

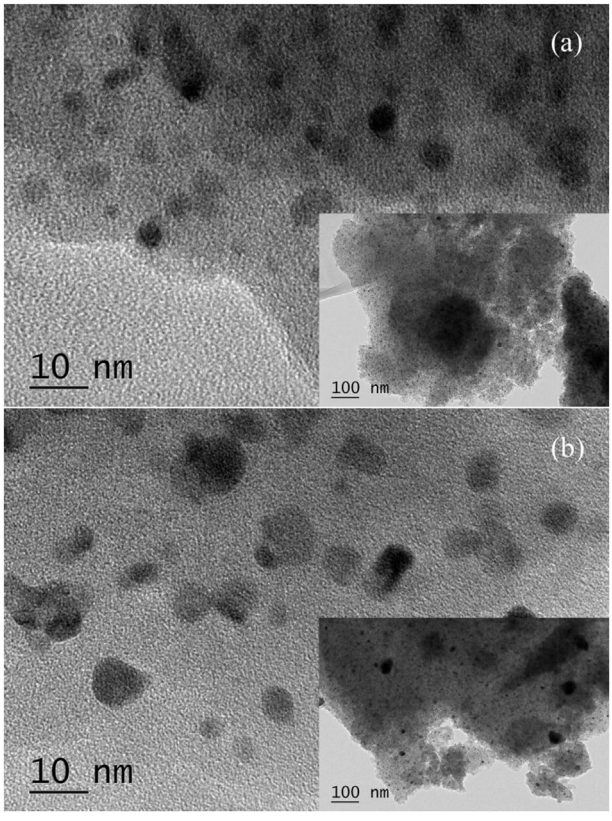

Fig. 1. TEM images of the POS powders calcined in (a) N_2 and (b) steam atmospheres at 400 °C.

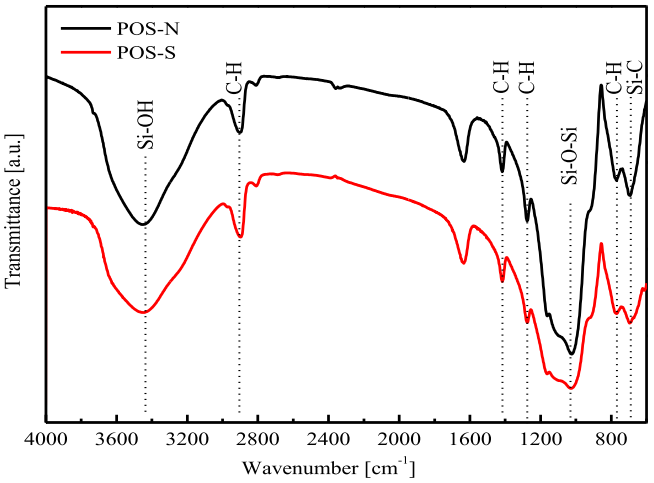

Fig. 2. FTIR spectra of the POS-N and POS-S powders.

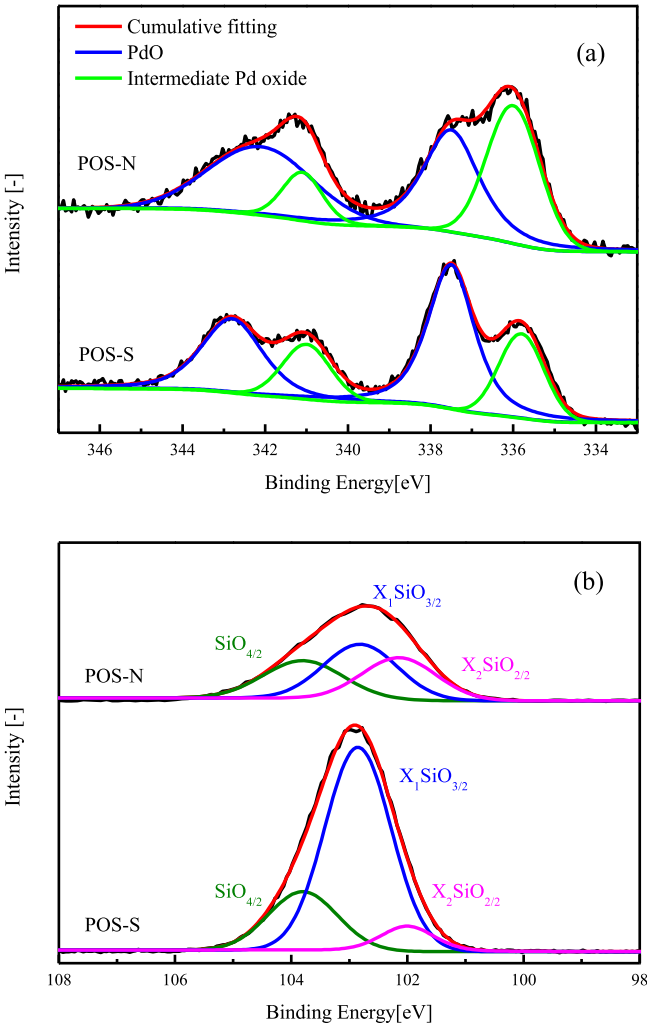

Fig. 3. (a) Pd 3d and (b) Si 2p spectra of the POS-N and POS-S powders in XPS analysis.

Fig. 3 describes the Pd 3d and Si 2p spectra of the POS-N and POS-S powders in XPS analysis. The two core-level peaks correspond to the $3d_{5/2}$ (336–337.5 eV) and $3d_{3/2}$ (341–343 eV) binding energy peaks of palladium. It is well known that the $3d_{5/2}$ binding energy values of ionic Pd^{2+} and metallic Pd are 338 and 335 eV, respectively [33]. However, the $3d_{5/2}$ binding energy peaks in Fig. 3a are between 335 and 338 eV which means the intermediate Pd oxide appeared. To further understand the chemical state of palladium, the binding energy peaks were deconvoluted by a software (XPSPEAK41). The core-level peaks of Pd $3d_{5/2}$ can be decoupled into two peaks, corresponding to PdO (337.5 eV) and intermediate Pd oxides (336 eV) [34]. Part of ionic Pd^{2+} is oxidized at high temperature. As a result, the binding energy peaks of PdO are observed in Fig. 3a. Appearance of the intermediate Pd oxides is an interesting phenomenon. This may be caused by the formation of covalent bonded palladium with hybrid silica networks. Similar structures have been observed in other metal doped silica systems [21,25]. The POS-S powders have much higher PdO but lower intermediate Pd oxide contents compared with the POS-N powders (Table 1).

In Fig. 3b, the Si 2p peaks can be decoupled into three peaks corresponding to $X_2SiO_{2/2}$ (102 eV), $XSiO_{3/2}$ (102.8 eV) and $SiO_{4/2}$ (103.7 eV) [35], where X represents organic groups in organosilica. The presence of the pure inorganic moiety ($SiO_{4/2}$) indicates pyrolysis of some organic bridges. The contents of the pure inorganic moiety and $X_2SiO_{2/2}$ in the POS-N powders are higher than those in the POS-S powders, while the content of $XSiO_{3/2}$ in the POS-N powders is lower than that in the POS-S powders (Table 1). Both FTIR and XPS analysis suggest the organic-inorganic hybrid structures of POS are formed after calcination in N_2 and steam atmospheres. However, the quantitative XPS analysis indicates the calcination atmosphere has a significant influence on chemical compositions of the POS powders.

Porous structures of the POS membranes are evaluated by the N_2 adsorption-desorption method (Fig. 4). The type I N_2 adsorption-desorption isotherms confirmed that the both POS samples have microporous structures which match with the previously reported structure of POS powders [36]. The specific surface areas of POS powders were calculated by the Brunauer–Emmett–Teller (BET) method. The POS-N sample has a BET surface area of 547.37 $m^2 \cdot g^{-1}$ and a pore volume of 0.31 $cm^3 \cdot g^{-1}$, while the POS-S sample has a smaller BET surface area (489.64 $m^2 \cdot g^{-1}$) and a smaller pore volume (0.29 $cm^3 \cdot g^{-1}$). This suggests that the POS-S membrane has a denser structure than the POS-N membrane.

It is worth noting that both POS-N and POS-S powders have negligible hysteresis loops (Fig. 4a), suggesting a few fractions of mesopores in the POS membranes. The presence of mesopores is confirmed by the pore size distributions of the POS-N and POS-S powders (Fig. 4b) based on the nonlocal density functional theory (NLDFT) [37]. In Fig. 4b, the pore size is mainly distributed in the range of 0.53–0.74 nm, the POS-N powder has similar microporosity compared with that of POS-S. This may lead to a close gas selectivity for the POS-N and POS-S membrane. Moreover, some mesopores are clearly observed and it explains the detectable permeances of SF_6 (d_k = 5.5 Å) for both POS-N and POS-S membranes.

Table 1
XPS analysis of the POS-N and POS-S powders before and after hydrothermal treatment.

Chemical state	[a] BE (eV)	POS-N		POS-S	
		Percentage (%)		Percentage (%)	
		Before	After	Before	After
PdO	337.5	50.3	19.3	69.3	98.3
[b] PdO_x	336.0	49.7	80.7	30.7	1.7
$SiO_{4/2}$	103.8	31.6	21.1	21.3	20.3
[c] $XSiO_{3/2}$	102.9	37.8	71.0	70.8	71.4
$X_2SiO_{2/2}$	102.0	30.6	7.9	7.9	8.3

[a] BE = Binding energy.
[b] PdO_x = Intermediate Pd oxide.
[c] X represents organic groups in organosilica.

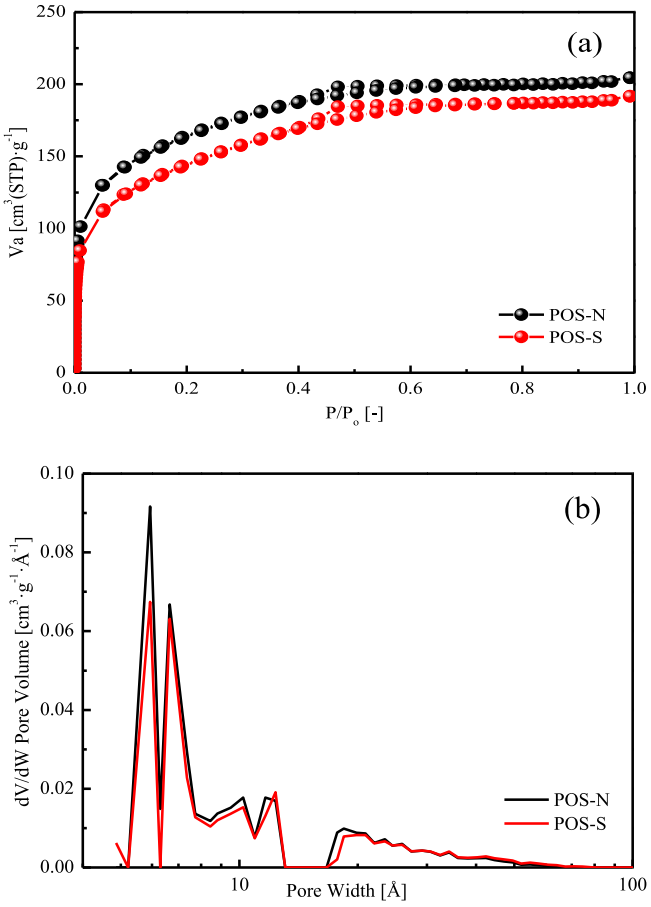

Fig. 4. (a) N_2 adsorption-desorption isotherms and (b) pore size distributions of the POS-N and POS-S powders.

3.2. POS membrane characterization

Fig. 5 shows the cross-sectional SEM images of (a) POS-N and (b) POS-S membranes. The POS membranes contain three layers, i.e. a α-Al_2O_3 macroporous support, a γ-Al_2O_3 mesoporous intermediate layer and a POS layer. The layered structure in POS-N and POS-S membrane could be clearly observed, and the thickness of the selective layers is about 150 nm.

The two membranes (POS-N and POS-S) have higher permeances to H_2 than other gases, indicating the excellent H_2 permselectivities (Fig. 6). The POS-S membrane shows a H_2 permeance of 2.5×10^{-7} $mol \cdot m^{-2} \cdot s^{-1} \cdot Pa^{-1}$, while the POS-N membrane has a smaller H_2 permeance of 1.1×10^{-7} $mol \cdot m^{-2} \cdot s^{-1} \cdot Pa^{-1}$. SF_6 permeances (2.5×10^{-9} $mol \cdot m^{-2} \cdot s^{-1} \cdot Pa^{-1}$ for the POS-S membrane, 4.1×10^{-9} $mol \cdot m^{-2} \cdot s^{-1} \cdot Pa^{-1}$ for the POS-N membrane) suggest that the two membranes contain some pores larger than 5.5 Å (Fig. 6a). This is in accordance with the results of pore size distribution in Fig. 4b.

The POS-N and POS-S membranes exhibit outstanding molecule sieving properties as the H_2 permselectivities of the membranes are

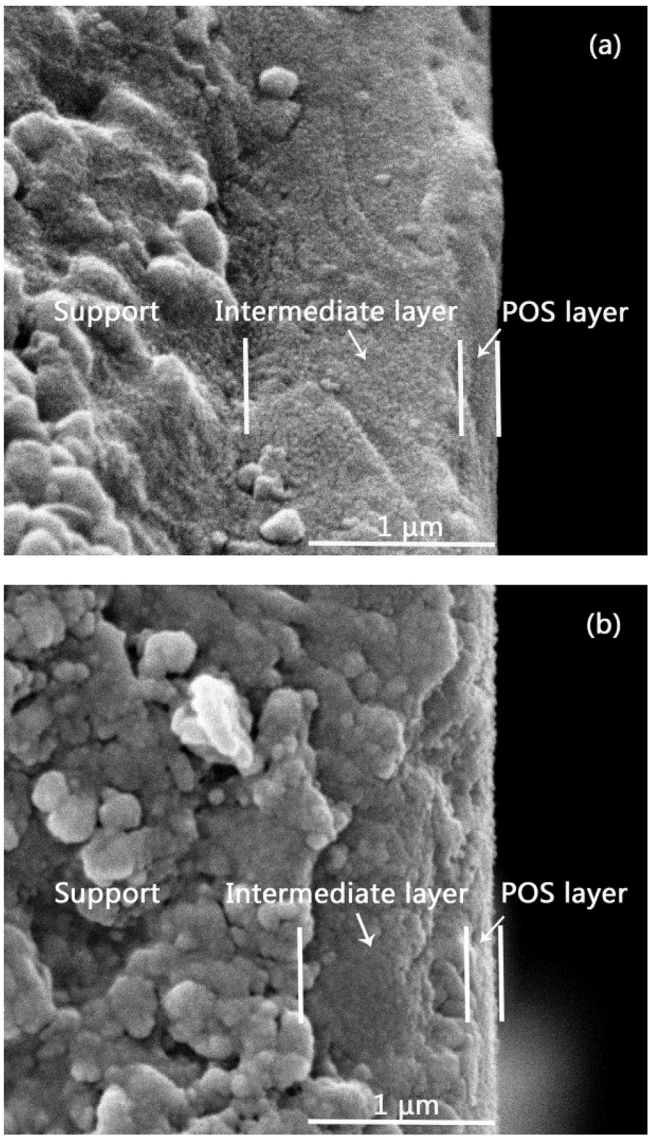

Fig. 5. Cross sectional SEM images of the (a) POS-N and (b) POS-S membrane.

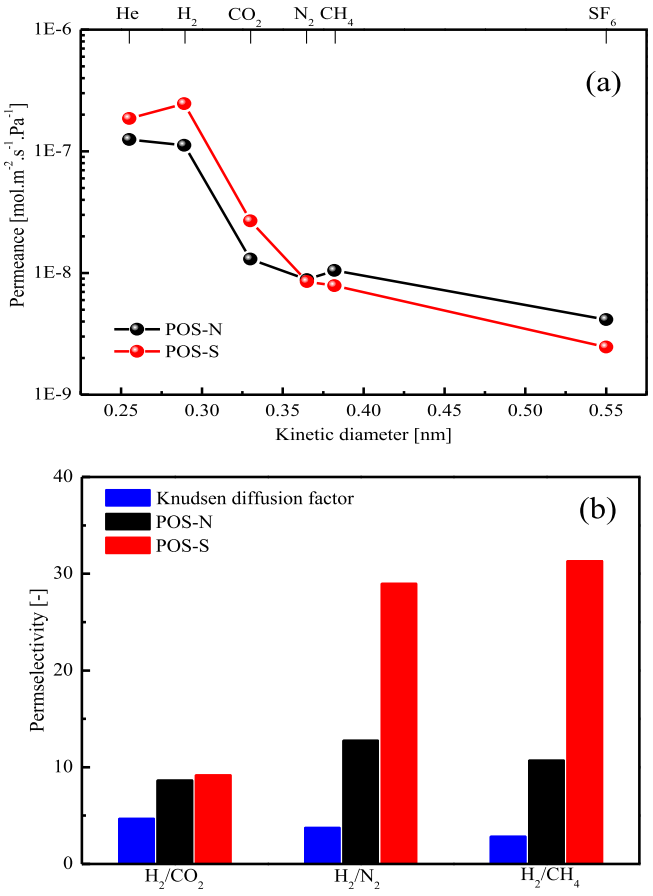

Fig. 6. (a) Single gas permeances and (b) permselectivities of the POS-N and POS-S membrane measured at 200 °C.

higher the corresponding Knudsen diffusion factors (Fig. 6b). Table 2 shows performance comparison of the POS-N and POS-S membrane by different detection method. The POS-S membrane shows high H_2/CO_2 selectivity of 33.5, and that of the POS-N is 25.1, which is obtained by separating the H_2/CO_2 gas mixture. Meanwhile, Single gas permeance test demonstrates that the H_2/CO_2 permselectivities of the POS-S and POS-N membrane are 9.2 and 8.6, respectively. Moreover, the H_2/CO_2, H_2/N_2 and H_2/CH_4 permselectivities of the POS-S membrane are also higher than those of the POS membrane calcined in reductive atmosphere (a gas mixture of H_2 and N_2) [24]. Obviously, calcination atmosphere plays an important role in membrane performance and the POS membrane calcined in steam atmosphere shows better molecule sieving properties.

3.3. Hydrothermal stability

H_2/CO_2 separation is mainly coupled with MSR and WGS reactions, where membranes inevitably contact water vapor at elevated temperature and high pressure [38, 39]. Thus, desirable membranes for H_2/CO_2 separation should have excellent hydrothermal stability apart from high permeance and selectivity.

Fig. 7 demonstrates the changes in gas permeance and permselectivity of the POS-N and POS-S membrane during hydrothermal treatments. H_2 and CO_2 permeances of the POS-N membrane increase gradually with the steam exposure time. After 40-h hydrothermal treatment, the H_2 permeance rises from 1.1×10^{-7} to 2.3×10^{-7} $mol \cdot m^{-2} \cdot s^{-1} \cdot Pa^{-1}$ and the H_2/CO_2 permselectivity declined to 4.7, which is approximately equal to the Knudsen diffusion factor (4.69). The H_2 and CO_2 permeances approach to a steady state value after 100 h. This suggests that the microstructure of the POS-N membrane has been totally destroyed in hydrothermal treatments. However, the POS-S membrane shows a very stable H_2 permeance (~2.7×10^{-7} $mol \cdot m^{-2} \cdot s^{-1} \cdot Pa^{-1}$) and H_2/CO_2 permselectivity (~10) throughout the 190-h hydrothermal treatment period.

Table 3 presents the performance comparison in terms of hydrothermal stability of the POS membranes with other silica-based membranes reported in literature [22, 25, 30, 40, 41]. It can be found that the pure silica membrane was unstable under hydrothermal conditions as the H_2 permeance decreased by 50% when the silica membrane was exposed to steam (partial pressure: 56 kPa) for 70 h. Most membranes also showed reductions in gas permeance after hydrothermal treatment, although some (i.e. Pd-SiO_2 and Pd-SiO_2, Ni-SiO_2 and Nb-BTESE) had improved permselectivities due to the more significant reduction of corresponding gas permeance. However, our POS-S membrane maintains steady gas permeance and permselectivity for 190 h, suggesting that the

Table 2
Performance comparison of the POS-N and POS-S membrane by different detection methods.

Membranes	H_2 permeance ($\times 10^{-7}$mol·m^{-2}·s^{-1}·Pa^{-1})		H_2/CO_2 permselectivity	H_2/CO_2 selectivity
	Single gas	Mixture gas		
POS-N	1.1	0.36	8.6	25.1
POS-S	2.5	0.58	9.2	33.5

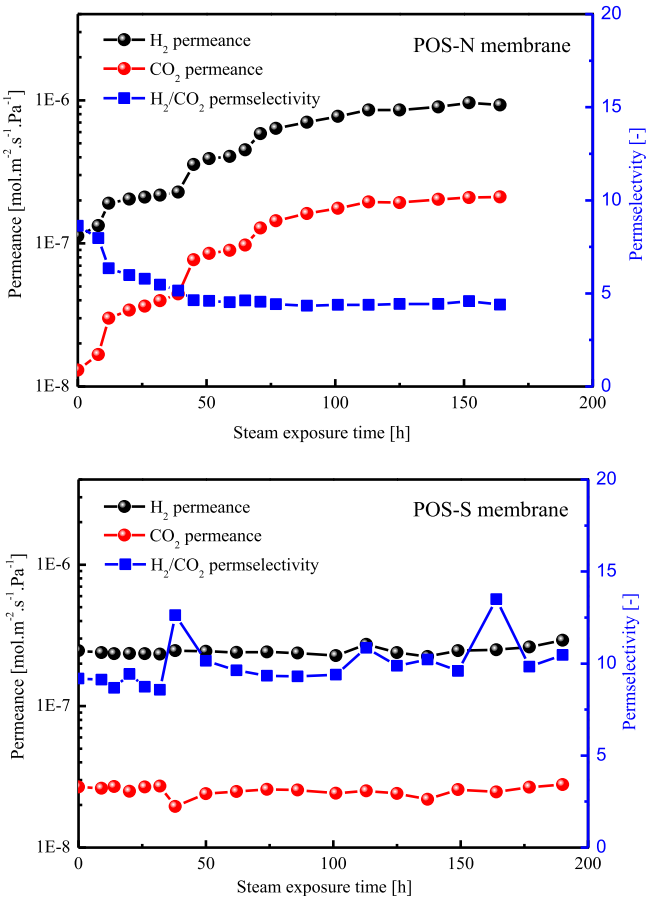

Fig. 7. Gas permeance and permselectivity changes of the POS-N and POS-S membrane after hydrothermal treatment.

prepared POS-S membrane is more promising in practical H_2 separation.

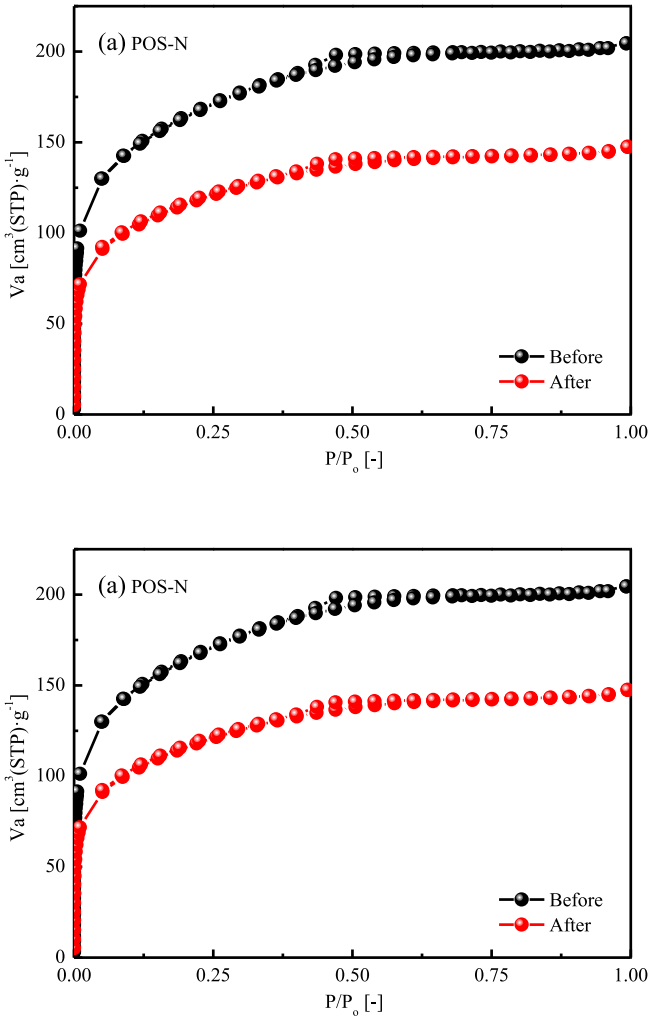

Fig. 8. N_2 adsorption-desorption isotherms of the POS powders before and after hydrothermal treatment.

Table 3
Performance comparison in terms of hydrothermal stability of silica-based membranes.

Membranes	Calcination conditions			H_2 permeance ($\times 10^{-7}$mol·m^{-2}·s^{-1}·Pa^{-1})		Permselectivity		Hydrothermal treatment conditions		
	[a]At	[b]T (°C)	[c]t (h)	[d]Before	[e]After	[d]Before	[e]After	[b]T (°C)	[c]t (h)	[f]P (kPa)
SiO_2 [40]	Air	500	3	6.3	3.1	46 (H_2/CO_2)	33 (H_2/CO_2)	150	70	56
Co-SiO_2 [41]	Air	630	2.5	2.5 (He)	1.1 (He)	50 (He/N_2)	39 (He/N_2)	550	40	70
Nb-BTESE [25]	N_2	450	3	0.6	0.2	120 (H_2/CO_2)	1500 (H_2/CO_2)	200	~ 10	150
Pd-SiO_2 [22]	H_2	400 (1st step)	1	6.0	5.0	100 (H_2/N_2)	260 (H_2/N_2)	500	~ 8	70
		550 (2nd step)	1							
Ni-SiO_2 [30]	Steam	550	0.5–1	10.3	4.1	160 (H_2/N_2)	482 (H_2/N_2)	500	60	70
Pd-BTESE (this work)	N_2	400	3	1.1	3.6	8.6 (H_2/CO_2)	4.6 (H_2/CO_2)	200	45	100
Pd-BTESE (this work)	Steam	400	3	2.5	2.6	9.2 (H_2/CO_2)	9.7 (H_2/CO_2)	200	190	100

[a] At = Atmosphere.
[b] T = Temperature.
[c] t = Time.
[d] Before = Before hydrothermal treatment.
[e] After = After hydrothermal treatment.
[f] P = Steam partial pressure.

To further explore the hydrothermal stability mechanisms of the POS membranes, N_2 adsorption-desorption isotherms, FTIR and XPS measurements were conducted for the corresponding powders that were hydrothermally treated for 24 h. N_2 adsorption-desorption isotherms of the POS powders confirm the excellent hydrothermal stability of the POS-S membrane (Fig. 8). After hydrothermal treatment, the BET surface area of the POS-N powders decreased 28.09% of its initial value drastically from 547.37 to 393.62 $m^2 \cdot g^{-1}$, while the BET surface area of the POS-S powders declined from 489.64 to 420.54 $m^2 \cdot g^{-1}$. The decrease ratio is only 14.16%, which is around the half of the ratio for POS-N membrane case. The pore volume of the POS-S decreased 10.34% from 0.29 to 0.26 $cm^3 \cdot g^{-1}$, while the pore volume of POS-N declined 25.81%. This indicates that the pore structure of the POS-S membrane is more stable than that of the POS-N membrane. Besides, FTIR spectras of the POS-N powders obviously changed (Fig. 9a) after hydrothermal treatment, while those of the POS-S powders were almost identical before and after hydrothermal treatment (Fig. 9b). This suggests that there is no significant change in chemical structure of the POS-S powders under hydrothermal conditions.

For the POS-N powders, their contents of silica after hydrothermal treatment change obviously (Table 1). For example, the

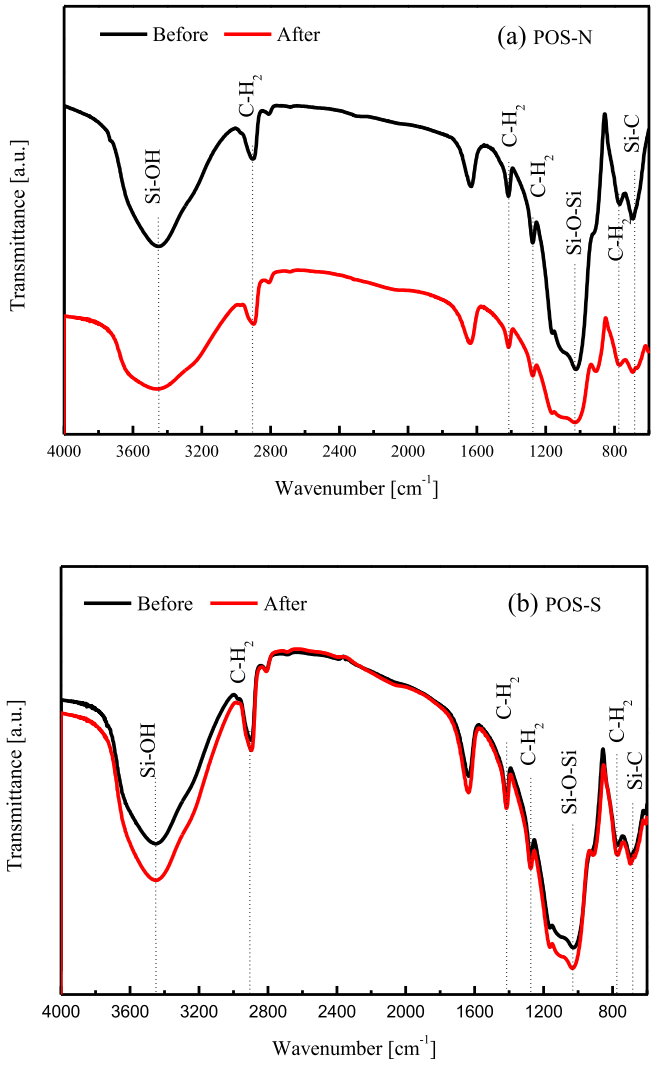

Fig. 9. FTIR spectra of the POS powders before and after hydrothermal treatment.

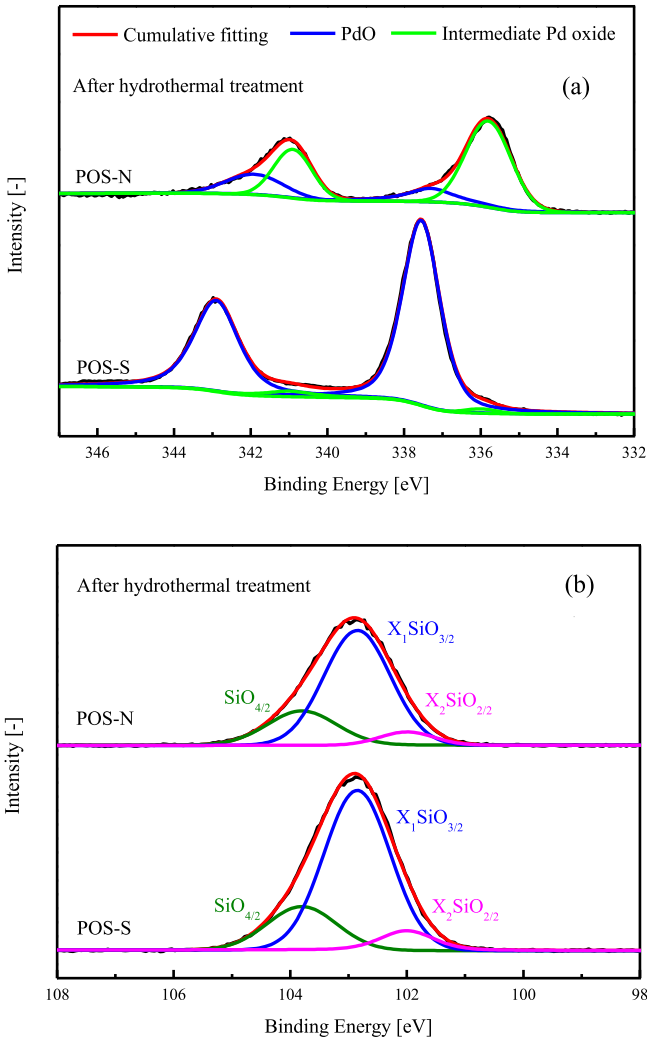

Fig. 10. (a) Pd 3d spectra and (b) Si 2p spectra of the POS-N and POS-S powders before and after hydrothermal treatment in XPS analysis.

content of unstable inorganic silica $SiO_{4/2}$ reduces from 31.6% to 21.1% after hydrothermal treatment. However, silica contents in the POS-S powders are almost unchanged. The POS-N and POS-S powders reach similar contents of silica after hydrothermal treatment (e.g. ~ 21%, 71% and 8% for $SiO_{4/2}$, $XSiO_{3/2}$, and $X_2SiO_{2/2}$ contents, respectively) (Fig. 10b and Table 1).

On the one hand, the high hydrothermal stability of the POS-S membrane is mainly attributed to the low content of unstable moieties in the POS network during steam calcination. For example, the unstable intermediate Pd oxide is transferred into stable PdO in POS-S network. It is well known that pure silica containing Si-O-Si groups is unstable under hydrothermal conditions [19, 42]. The Si-O-Si groups in the POS-S network are first decomposed when encountering water molecules at high temperature. The generated mobile silanol groups could depart from the matrix in the steam calcination process. As a consequence, the POS-S membrane has relatively low content of inorganic moieties, which makes the POS-S membrane more stable under hydrothermal conditions. Structure evolutions of the two POS membranes in hydrothermal treatment are illustrated in Fig. 11.

On the other hand, quantitative XPS analysis shows that the POS-N powders have a higher content of intermediate Pd oxide (49.7% vs 30.7%), while the POS-S powders have a higher content of

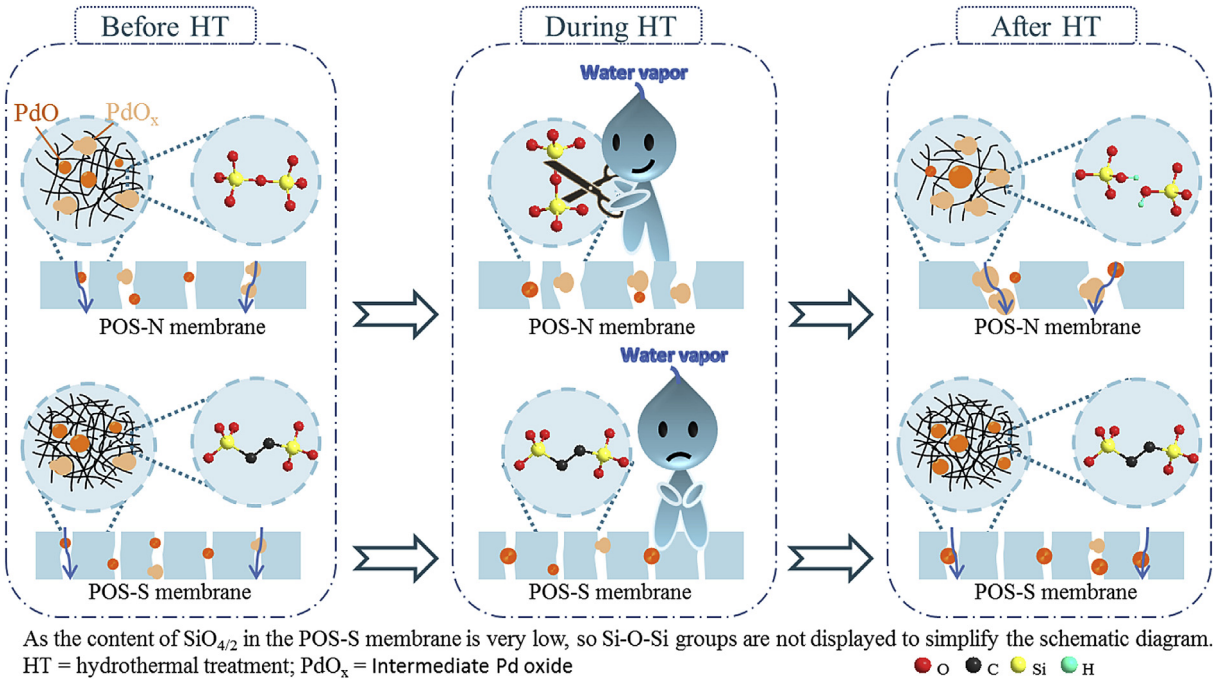

Fig. 11. Schematic comparison of structure evolution of the POS membranes in hydrothermal treatment.

Table 4
The grain size of Pd in the POS-N and POS-S powders before and after hydrothermal treatment obtained from XRD.

Samples	Grain size/nm		Increase ratio/%
	Before	After	
POS-N	5.99	28.50	375.80
POS-S	14.62	20.10	37.48

PdO (69.3% vs 50.3%) before hydrothermal treatment (Table 1). After hydrothermal treatment, the moiety of hydrothermally stable PdO in the POS-N powders is decreased to 19.3%, while the moiety of unstable intermediate Pd oxide in POS-S is transferred into stable PdO (98.3%) from Fig. 10a and Table 1. Intermediate Pd oxide transformed into more stable PdO during steam atmosphere (Fig. 11).

In addition, doping metals into the matrix networks implies that the metal particles are dispersed in the channels of porous materials [43]. The chemical state and grain size of metal Pd have a great influence on the pore diameter and shape, which determines the gas permeability [44, 45]. The size of metal Pd in POS-S powders increased from 14.62 nm to 20.10 nm, showing little change before and after hydrothermal treatment, while it increased 375.80% of initial value in POS-N powders obtained from XRD by Scherrer formula (Table 4). Correspondingly, the H_2 permeance of POS-S maintained in a range of ~2.5 × 10^{-7}mol·m^{-2}·s^{-1}·Pa^{-1} after hydrothermal treatment for 190 h, however, the H_2 permeance of POS-N increased from 1.2 × 10^{-7} to 2.3 × 10^{-7} mol·m^{-2}·s^{-1}·Pa^{-1} after only 40 h. It was confirmed that the POS-S showed less change in the network matrix, chemical state, grain size of metal Pd in steam atmosphere, which contributed to the more stable permeance of the POS-S in hydrothermal atmosphere, namely, higher hydrothermal stability of POS-S membranes.

4. Conclusions

The POS membrane calcined in steam atmosphere exhibits good hydrogen separation performance (H_2 permeance 2.5 × 10^{-7} mol·m^{-2}·s^{-1}·Pa^{-1}; H_2/CO_2 permselectivity 9.2) and excellent hydrothermal stability. Although calcination in N_2 and steam lead to similar chemical bonds in the microporous POS networks, chemical compositions of the POS-N and POS-S membranes are different. The POS-S membrane has a lower content of inorganic moieties and intermediate Pd oxide than the POS-N membrane, resulting in excellent hydrothermal stability. The POS-S membrane can maintain its high H_2 permeance and permselectivity for up to 190 h under hydrothermal conditions, which outperforms most silica-derived membranes. Water vapor makes unstable intermediate Pd oxide transfer into stable PdO and decrease content of inorganic moieties during the calcination, leading to high hydrothermal stability of the POS-S membrane. Therefore, calcination in steam atmosphere may offer an effective strategy to develop desirable silica-based membranes with high separation performances and excellent hydrothermal stabilities for practical hydrogen separation.

Acknowledgements

This study is supported by the National Natural Science Foundation of China (21276123, 21490581), the National High Technology Research and Development Program of China (2012AA03A606), the “Summit of the Six Top Talents” Program of Jiangsu Province (2011-XCL-021), and the Open Research Fund Program of Collaborative Innovation Center of Membrane Separation and Water Treatment (2016YB01).

References

[1] Y.W. Budhi, H. Rionaldo, A.A.B. Padama, H. Kasai, I. Noezar, Int. J. Hydrogen Energy 40 (2015) 10081–10089.

[2] D. Georgis, F.V. Lima, A. Almansoori, P. Daoutidis, Ind. Eng. Chem. Res. 53 (2014) 7461–7469.
[3] Hydrogen Production: Natural Gas Reforming, U.S. Office of Energy Efficiency & Renewable Energy, 2016. https://energy.gov/eere/fuelcells/hydrogen-production-natural-gas-reforming.
[4] S.J. Kim, S. Yang, G.K. Reddy, P. Smirniotis, J. Dong, Energy Fuel 27 (2013) 4471–4480.
[5] H. Li, K. Haas-Santo, U. Schygulla, R. Dittmeyer, Chem. Eng. Sci. 127 (2015) 401–417.
[6] H. Yin, T. Lee, J. Choi, A.C.K. Yip, Microporous Mesoporous Mater 233 (2015) 70–77.
[7] Z. Jia, G. Wu, Microporous Mesoporous Mater 235 (2016) 151–159.
[8] Y. Zhang, X. Feng, S. Yuan, J. Zhou, B. Wang, Inorg. Chem. Front. 3 (2016).
[9] K. Huang, S. Liu, Q. Li, W. Jin, Sep. Purif. Technol. 119 (2013) 94–101.
[10] Y. Peng, Y. Li, Y. Ban, H. Jin, W. Jiao, X. Liu, W. Yang, Science 346 (2014).
[11] H. Yin, H. Kim, J. Choi, A.C.K. Yip, Chem. Eng. J. 278 (2015) 293–300.
[12] Y. Zhang, X. Feng, S. Yuan, J. Zhou, B. Wang, Inorg. Chem. Front. 3 (2016).
[13] J. Shen, G. Liu, K. Huang, Z. Chu, W. Jin, N. Xu, Acs Nano 10 (2016) 3398.
[14] K. Guan, J. Shen, G. Liu, J. Zhao, H. Zhou, W. Jin, Sep. Purif. Technol. 174 (2016) 126–135.
[15] H.F. Qureshi, A. Nijmeijer, L. Winnubst, J. Membr. Sci. 446 (2013) 19–25.
[16] H.L. Castricum, A. Sah, R. Kreiter, D.H. Blank, J.F. Vente, J.E. ten Elshof, Chem. Commun. (2008) 1103–1105.
[17] M. Kanezashi, K. Yada, T. Yoshioka, T. Tsuru, J. Membr. Sci. 348 (2010) 310–318.
[18] H. Song, S. Zhao, J. Chen, H. Qi, Microporous Mesoporous Mater 224 (2016) 277–284.
[19] M. Kanezashi, K. Yada, T. Yoshioka, T. Tsuru, J. Membr. Sci. 348 (2010) 310–318.
[20] M.C. Duke, J.C.D. da Costa, D.D. Do, P.G. Gray, G.Q. Lu, Adv. Funct. Mater 16 (2006) 1215–1220.
[21] R. Igi, T. Yoshioka, Y.H. Ikuhara, Y. Iwamoto, T. Tsuru, J. Am. Ceram. Soc. 91 (2008) 2975–2981.
[22] M. Kanezashi, D. Fuchigami, T. Yoshioka, T. Tsuru, J. Membr. Sci. 439 (2013) 78–86.
[23] M. Kanezashi, M. Sano, T. Yoshioka, T. Tsuru, Chem. Commun. 46 (2010) 6171–6173.
[24] H. Song, S. Zhao, J. Lei, C. Wang, H. Qi, J. Mater Sci. 51 (2016) 6275–6286.
[25] H. Qi, H. Chen, L. Li, G. Zhu, N. Xu, J. Membr. Sci. 421–422 (2012) 190–200.
[26] J. Boon, J.A.Z. Pieterse, F.P.F. van Berkel, Y.C. van Delft, M. van Sint Annaland, J. Membr. Sci. 496 (2015) 344–358.
[27] X. Li, A. Li, C.J. Lim, J.R. Grace, J. Membr. Sci. 499 (2016) 143–155.
[28] K. Naga Mahesh, R. Balaji, K.S. Dhathathreyan, Int. J. Hydrogen Energy 41 (2016) 46–51.
[29] D. Gudarzi, W. Ratchananusorn, I. Turunen, M. Heinonen, T. salmi, Catal. Today 248 (2015) 69–79.
[30] M. Kanezashi, M. Asaeda, J. Membr. Sci. 271 (2006) 86–93.
[31] K. Yamamoto, J. Ohshita, T. Mizumo, T. Tsuru, J. Non-Cryst Solids 408 (2015) 137–141.
[32] H.F. Qureshi, R. Besselink, J.E. ten Elshof, A. Nijmeijer, L. Winnubst, J. Sol-Gel Sci. Technol. 75 (2015) 180–188.
[33] B.D. Mukri, G. Dutta, U.V. Waghmare, M.S. Hegde, Chem. Mater 24 (2012) 4491–4502.
[34] K. Fujiwara, U. Müller, S.E. Pratsinis, ACS Catal. 6 (2016) 1887–1893.
[35] P.H.T. Ngamou, J.P. Overbeek, R. Kreiter, H.M. van Veen, J.F. Vente, I.M. Wienk, P.F. Cuperus, M. Creatore, J. Mater Chem. A 1 (2013) 5567.
[36] M. Thommes, K. Kaneko, A.V. Neimark, J.P. Olivier, F. Rodriguez-Reinoso, J. Rouquerol, K.S.W. Sing, Pure Appl. Chem. 87 (2015).
[37] M. Wei, L. Zhang, Y. Xiong, J. Li, P. a. Peng, Microporous Mesoporous Mater 227 (2016) 88–94.
[38] M. Gonzalez Castaño, T.R. Reina, S. Ivanova, M.A. Centeno, J.A. Odriozola, J. Catal. 314 (2014) 1–9.
[39] F. Gallucci, E. Fernandez, P. Corengia, M. van Sint Annaland, Chem. Eng. Sci. 92 (2013) 40–66.
[40] V. Boffa, D. Blank, J. Tenelshof, J. Membr. Sci. 319 (2008) 256–263.
[41] L. Liu, D.K. Wang, D.L. Martens, S. Smart, J.C. Diniz da Costa, J. Membr. Sci. 475 (2015) 425–432.
[42] J. Wang, G. Gong, M. Kanezashi, T. Yoshioka, K. Ito, T. Tsuru, J. Membr. Sci. 441 (2013) 120–128.
[43] M. Kanezashi, M. Sano, T. Yoshioka, T. Tsuru, Chem. Commun. 46 (2010) 6171–6173.
[44] B. Ballinger, J. Motuzas, S. Smart, J.C. Diniz da Costa, J. Membr. Sci. 451 (2014) 185–191.
[45] Q. Wei, F. Wang, Z.R. Nie, C.L. Song, Y.L. Wang, Q.Y. Li, J. Phys. Chem. B 112 (2008) 9354–9359.